Urban-climate interactions during summer over eastern North America

Seok-Geun Oh (poet1535@gmail.com)
Seoul National University https://orcid.org/0000-0001-7496-9402
Laxmi Sushama
McGill University

Research Article

Keywords: urban-climate interactions, regional climate model, precipitation extremes, heat-stress conditions

Posted Date: June 7th, 2021

DOI: https://doi.org/10.21203/rs.3.rs-330727/v1

Abstract

The urban heat island is a representative urban climate characteristic, which can affect heat-stress conditions and extreme precipitation that are closely connected with human life. Better understanding of urban-climate interactions, therefore, is crucial to ultimately support better planning and adaptation in various application fields. This study assesses urban-climate interactions during summer for eastern North America using regional climate model simulations at 0.22° resolution. Two regional climate model experiments, with and without realistic representation of urban regions, are performed for the 1981–2010 period. Comparison of the two experiments shows higher mean temperatures and reduced mean precipitation in the simulation with realistic urban representation, which can be attributed primarily to reduced albedo and soil moisture for the urban regions in this simulation. Furthermore, the mean temperature and precipitation in the simulation with improved urban representation is also closer to that observed. Analysis of short-duration precipitation extremes for climatologically different sub-regions, however, suggests that, for higher temperatures, the magnitudes of precipitation extremes are generally higher in the simulation with realistic urban representation, particularly for coastal urban regions, and are collocated with higher values of convective available potential energy and cloud fraction. Enhanced sea and lake breezes associated with lower sea level pressure found around these regions, contribute additional water vapor and further enhance dynamic convective development, leading to higher precipitation intensities. Analysis of temperature extremes clearly demonstrates that urban regions experience aggravated heat-stress conditions due to relatively higher temperatures despite reduced relative humidity. Double the number of extreme heat spells lasting six or more days are noted for the coastal urban regions in the study domain. This study, in addition to demonstrating the differences in urban-climate interactions for climatologically different regions, also demonstrates the need for better representation of urban regions in climate models to generate realistic climate information.

1. Introduction

Urban regions modify regional weather and climate, as they are anthropogenic heat and aerosols sources, a meager storage system for water and an obstruction to atmospheric motion (e.g., Oke 1982; Huszar et al. 2014; Daniel et al. 2019). The urban heat island (UHI), which represents higher temperatures in urban regions than their surrounding non-urban/rural areas, can further augment extreme temperature events leading to severe heat-stress conditions (e.g., Oleson et al. 2015; Daniel et al. 2019). In addition, the UHI may also contribute to strengthening convection which can lead to precipitation extremes (e.g., Shepherd and Burian 2003; Molders and Olson 2004; Wang et al. 2015). Better understanding of urban-climate interactions, therefore, is crucial in establishing effective countermeasures to safety and security issues caused by extreme weather and climate events for the urban regions.

Many recent global climate modeling studies (e.g. McCarthy et al. 2010; Oleson et al. 2011; Oleson 2012) have focussed on urban-climate interactions, as the urban-induced warming besides greenhouse gas-induced warming has not explicitly been considered in climate change simulations (IPCC 2007). For example, Oleson et al. (2011) reported that the parameterization for urban surface properties incorporated

into the Community Climate System Model (CCSM) permits global simulation of the urban environment, particularly the UHI phenomenon. They showed that the average UHI for all urban regions resolved in the model is around 1.1ºC, which is 46 % of the greenhouse gas-induced global warming projected over land by mid-century. They, therefore, suggested that it is crucial to include urban representations in global climate model simulations. Despite these efforts, urban surfaces are not adequately represented in many global climate models, primarily because of their coarser resolution.

Regional climate models, a dynamic downscaling approach, have been popularly used in order to produce high-resolution regional weather and climate, as they 'add details' to global climate model simulations (e.g., Cha et al. 2016; Jeong and Sushama 2016; Teufel et al. 2017; Oh and Sushama 2020). Furthermore, with increasing computing resources, it has become possible to implement high-resolution simulations with regional climate models with improved urban surface parameterization that represents explicitly the impacts of various urban components such as roof, wall, and road, etc. (e.g., Bélair et al. 2018; Karlicky et al. 2018; Daniel et al. 2019). For example, Bélair et al. (2018) investigated the effects of urban surfaces on an extreme precipitation event in Tokyo during August 2010, and found that urban regions enhanced the lateral inflow of moist static energy from the Tokyo Bay, leading to increased precipitation intensity. Daniel et al. (2019) evaluated the added value of a sophisticated urban canopy scheme compared to a simpler approach over France using regional climate model simulations spanning the 1980–2009 period. They noted improvements in the diurnal cycle of surface 2-m temperature, primarily due to the ability in capturing better the nighttime temperature warming. These studies both reported the added-value of the regional climate model coupled with the urban canopy scheme in simulating the mean climate and extreme events for the respective analysis region and suggested the importance of the use of a coupled modeling for understanding the urban climate systems.

The goal of this study, therefore, is to assess urban-climate interactions over eastern North America using regional climate model simulations, with and without the urban canopy scheme, for the 1981–2010 period. It is also the aim to assess the effects of urban environment on extreme weather/climate events such as short-duration precipitation extremes and heat-stress conditions and to investigate associated mechanisms. This study is the first step for long-term urban climate change scenario analyzes and will provide baseline information to assess projected changes induced by urban effects, in addition to greenhouse gas-induced climate change scenarios, which can inform better planning and adaptation strategies in various fields.

The rest of the paper is composed as follows. Section 2 explains the regional climate model, the urban canopy scheme, and the experimental design and methodology used in this study. Section 3 presents comparison results of regional climate simulations with and without the urban canopy scheme for mean climate and investigates the added-value of coupled simulation through comparison with observation. In addition, the effects of urban regions on extreme weather/climate events and associated mechanisms are also discussed. Summary and conclusion are presented in Sect. 4.

2. Model And Experimental Design

2.1 Regional climate model

This study uses the limited area version of the Global Environmental Multiscale (GEM) model of Environment and Climate Change Canada (ECCC, Cote et al. 1998; Yeh et al. 2002). The GEM has a non-hydrostatic dynamic core and uses Arakawa C grid staggering in the horizontal and a hybrid terrain-following vertical coordinate. It employs a two-time-level semi-Lagrangian implicit scheme. In this study, deep convection of Kain and Fritsch (1992), shallow convection of Bélair et al. (2005), and resolvable large-scale precipitation of Sundqvist et al. (1989) are used. Radiation is computed by Correlated-K solar and terrestrial radiation (Li and Barker 2005). The planetary boundary layer parameterization suggested by Benoit et al. (1989) and Delage (1997), with modifications from Zadra et al. (2012), is used. The land surface scheme used is the Canadian land-surface scheme (CLASS, Verseghy 2009) version 3.5, which has been used and evaluated in many previous studies (e.g., Teufel et al. 2017). CLASS has a flexible soil layering scheme and prognostically calculates energy and water conservation. In addition, it uses a thermally and hydrologically distinct snowpack, which is handled as an additional variable-depth soil layer. In this study, CLASS is configured with 26 levels reaching a total depth of 10 m. In CLASS, the thermal budget is calculated for all soil layers but the hydrological budget is only calculated for layers above bedrock. For urban regions, CLASS considers them as bare soil with a high roughness length. Therefore, this study uses Town Energy Balance (TEB, Masson 2000) scheme to represent urban-climate interaction, realistically. More details of the TEB scheme are discussed below. For representing lakes, the one-dimensional Flake model (Martynov et al. 2013) is used.

The Town Energy Balance (TEB) scheme, developed by Masson (2000), is based on the mean urban canyon approach (Oke 1988), and consists of elementary surfaces, such as roof, road, and walls, and uses mean geometric parameters such as building density and height and mean thermal and radiative properties and street aspect ratio. TEB simulates prognostically the evolution of roof, wall, and road temperatures from the calculation of individual surface energy budgets including heat diffusion transfer. Street orientation is assumed to be isotropic and trapping effects are considered in radiative forcing. Turbulent exchanges in urban-atmosphere interaction are represented over roofs and urban canyons according to wind speed and stability conditions. The TEB scheme has been extensively evaluated over various cities and climatic conditions (e.g., Masson et al. 2002; Hamdi et al. 2012; Leroyer et al. 2011; Roberge and Sushama 2018). Several studies have been performed with GEM coupled with TEB as well (e.g., Bélair et al. 2018), but for short durations.

2.2 Experimental design and methodology

The model domain used in this study covers eastern North America and adjoining ocean (Fig. 1). It consists of 145 × 148 grid points at 0.22° horizontal resolution, and has 62 levels in the vertical. The European Centre for Medium-Range Weather Forecast (ECMWF) Re-Analysis (ERA)-Interim (Dee et al. 2011) is used as a lateral boundary condition to drive the GEM model. Two experiments, with and without TEB, are performed to investigate the urban-climate interactions over the domain for the 1981–2010 period. The simulations with and without TEB will be represented as GEM_TEB and GEM, respectively. For representing realistic land use and urbanization in GEM_TEB experiment, as shown in Fig. 1, the

pavement and building fractions are specified using recent information from OpenStreetMap (Bélair et al. 2018); the urban fraction is presented in Fig. 1 as the sum of the above two variables. For GEM_TEB simulation, TEB-specific parameters such as building height, canyon aspect ratio, roof (wall/road) albedo and emissivity, and roughness length, etc. are required. Urban-related parameters are estimated from Canadian Vector Data (CanVec) version 9.0 which is based on the National Topographic Database (NTDB), the Geobase initiative and radar imagery from Landsat 7, SPOT and Radarsat (Nazarnia et al. 2016; Roberge and Sushama 2018). The example of input parameters used in this study is presented in Table S1. The TEB scheme is active for the grids with urban fraction higher than 0. However, it must be noted that the temporal variation of land use including the development of urban areas are not considered in the simulation. Three subregions – coastal, inland and Great Lakes – located in climatologically different regions are chosen for detailed analysis, particularly to study the impact of geographic location/features on urban-climate interactions. In this study, only grid cells with urban fractions higher than 8% are used in the detailed analyses presented for subregions. Different thresholds have been used in previous studies. For example, Dainel et al. (2019), in their study using regional climate simulations with TEB for France, considered a 10% threshold. However, the use of lower urban fraction in this study is probably more appropriate as our model resolution, about 25 km, is coarser than the 12 km resolution of their model. Indeed, the model grids with urban fraction above 8% well represent the location of mega cities such as Philadelphia, Chicago, and Cincinnati for each subregion compared to the urban extent with 1 km resolution over eastern North America produced by the Global Rural-Urban Mapping Project version 1 (Balk et al., 2006), which is based on a combination of population counts (persons), settlement points, and the presence of nighttime lights (not shown).

All analyses presented in this study focus on the summer season (June, July, and August) when urban-climate interactions are more predominant. To assess the added-value of GEM_TEB for mean climate, model simulations are compared with Daymet version 3 daily gridded dataset, which accounts for elevation changes for both precipitation and temperature based on a Gaussian weighting filter centered at the observation locations with linear regression (Thornton et al., 2017). This observation covers whole of North America and provides a daily temporal resolution and a 1 km spatial resolution for the 1980 to 2016 period. The observed variables are interpolated to the model grid to facilitate comparison.

In this study, the model simulations are compared with respect to the following processes and mechanisms: (1) spatial and diurnal variations of surface 2-m temperature and precipitation and related surface energy fluxes, (2) short-duration precipitation extremes and related atmospheric fields, and (3) temperature extremes defined in terms of heat-stress characteristics (total number, duration, and start and end dates). The simulated surface 2-m temperature and precipitation are evaluated against observations and the differences of simulated surface energy fluxes are used to explain the differences between GEM_TEB and GEM. For short-duration precipitation extremes, the simulated precipitation-temperature (P-T) relationship is compared. The methodology suggested by Lenderink and van Meijgaard (2010) based on Clausius-Clapeyron relationship (CC scaling, hereafter), which assumes that extreme precipitation intensities are expected to increase by ~ 7 % per degree warming (ºC), is applied to the experiments. This study considers the 99th percentile of hourly precipitation intensities for each temperature bin as extreme

precipitation, and these calculations are conducted when the number of precipitation events (hourly precipitation intensity > 0.3 mm/h) for a given temperature bin is larger than 100. Temperature and precipitation fields from the fifth generation of ECMWF atmospheric reanalysis (ERA5, Hersbach et al. 2020), the spatial resolution of which is closer to that of the simulations considered in this study, are used to compare the simulated P-T curve for climatologically different sub-regions. In addition, various atmospheric fields (i.e., convective potential available energy, sea level pressure, surface wind, and cloud fraction) are also analyzed to understand the mechanisms associated with urban-induced short-duration precipitation extremes.

A heat-stress day in this study is defined as a day when apparent temperature exceeds a predefined threshold. The apparent temperature here is a perceived temperature measure that considers human physiology and the human body's ability to dissipate heat and has been widely used in the National Weather Forecast offices of the United States (Smoyer 1998; Steinweg and Gutowski 2015). Following Steadman (1984), apparent temperature (T_{app}, ºC), which is based on both 2-m temperature (T_a, ºC) and humidity as discussed above, is estimated as:

$$T_{app} = 2.719 + 0.994\ (T_a) + 0.016\ (T_d)^2.$$

Here, T_d is dew point temperature (ºC), estimated using 2-m specific humidity (g/kg). The threshold used to identify heat-stress days corresponds to the 90th percentile of apparent temperature for respective grid cells. To consider the seasonal cycle, a 15-day moving average is applied for each Julian day and then the smoothed 90th percentile thresholds are estimated (Jeong and Sushama 2016). The thresholds estimated from the GEM experiment are applied to both GEM and GEM_TEB outputs in detecting heat-stress days. In addition, a heat-stress event is defined as an extended period of heat-stress days; this can be of any duration including 1 day.

3. Results

3.1 Validation for urban-climate interaction on mean climate

Figures 2 and 3 show the observed and modelled mean summer surface 2-m temperatures (ºC) and precipitation (mm/day) for the 1981–2010 period. In general, the two experiments well reproduce the spatial distribution of observed surface 2-m temperature and precipitation. For surface 2-m temperature, the spatial correlation is 0.94 for GEM and GEM_TEB, suggesting that both simulations realistically capture the spatial temperature characteristics for this region induced by the differences in latitude, land cover, and topography. However, GEM shows warm temperature biases of about 0.5–1.5 ºC for most of the analysis domain and cold temperature biases of about 0.5–1.0 ºC for some parts of the coastal and Great Lakes regions. GEM_TEB simulated temperatures are higher for the urban regions by around 0.7 ºC compared to GEM, suggesting improvements for the grid cells with cold bias in the GEM experiment. However, for urban regions with warm biases in GEM, they are further enhanced in the GEM_TEB experiment. For precipitation, dry and wet biases in the 0.3–1.2 mm/day range can be noted for the

western and eastern regions, respectively, of the analysis domain in both experiments. Precipitation amounts in GEM_TEB are 0.3–0.5 mm/day smaller than that in GEM experiment, particularly for the eastern regions of the analysis domain. This reduced precipitation in GEM_TEB experiment appear not only in urban regions/cells but also in nearby grid cells, leading to improved performances for both precipitation magnitude and spatial correlation, compared to the GEM experiment. Therefore, these validation results suggest that GEM_TEB improves generally the mean climate characteristics for 2-m temperature (except for grid cells with temperature warm bias in GEM) and precipitation over the analysis domain compared to the GEM experiment, particularly for the urban cells.

Figure 4 analyzes the spatial distribution of the differences in albedo (%), sensible and latent heat fluxes (W/m^2), 2-m specific humidity (g/kg), evaporation (kg/m^2), and soil moisture (mm) for the 1981–2010 period to investigate the summer surface 2-m temperature and precipitation differences in the two experiments. Albedo in GEM_TEB for urban regions is about 1–3 % smaller than that in GEM. Higher (lower) sensible (latent) heat flux, over 20 W/m^2, is also noted for urban regions in GEM_TEB, as expected. The higher value of sensible heat flux is consistent with the lower albedo in GEM_TEB, which leads to higher absorbed solar radiation at the surface during daytime compared to the GEM experiment, and reduced latent heat flux associated with reduced soil moisture and therefore evaporation in GEM_TEB. This result is in good agreement with previous studies that looked at urban effects on surface albedo, sensible and latent heat fluxes (Miao et al. 2012; Huszar et al. 2014; Roberge and Sushama 2018; Daniel et al. 2019). No significant differences are noted between the two experiments in the wind fields (not shown), suggesting that the contribution of advection to the noted differences in precipitation is not significant. On the other hand, the 2-m specific humidity is about 0.3–0.6 g/kg smaller in GEM_TEB than in GEM, contributing to the lower precipitation amounts for the urban and surrounding non-urban/rural regions GEM_TEB (Fig. 4). This result is partly consistent with previous modeling studies (e.g., Li et al. 2016; Zhang et al. 2019), which reported that urban surfaces lead to reduced near-surface moisture and precipitation. However, it should be noted that some other studies (e.g., Karlický et al. 2020; Manola et al. 2020) have reported increases in precipitation due to more frequent thermal convection associated with atmospheric instability from the heated urban surfaces.

To investigate the varying effects of geographic locations on urban-climate interaction in detail, the differences in the diurnal cycle of surface 2-m temperature and other surface energy fluxes for three sub-regions are assessed in Fig. 5. Based on the surface energy balance equation, the residual term in this study is estimated as the difference between the net radiative and turbulent fluxes. Only grid cells with urban fractions above 8 % are used in the analysis. GEM_TEB temperatures are higher than that of GEM, with maximum differences found at nighttime (21–03 local standard time, LST) than daytime (09–15 LST). Interestingly, nighttime differences for the inland region are higher than that for the coastal and Great Lakes regions, and it may partly be attributed to the small size of the analysis area as well (Fig. 1). The diurnal cycles of absorbed solar radiation and downward longwave radiation for all sub-regions are slightly higher in GEM_TEB, with the largest positive difference of about 25 W/m^2 noted during 12–15 LST. This higher absorbed solar radiation in GEM_TEB is closely linked to the smaller albedo as shown in

Fig. 4. The higher downward longwave radiation is partly related to the trapping effects in the urban canyon (Masson et al. 2002). The warmer air above cities could also contribute to the higher downward longwave radiation.

The diurnal cycle of sensible (latent) heat flux is significantly enhanced (weakened) and shows the largest positive difference (negative difference) during 12–15 LST at 5 % significance level as per Student's t-test. It is noteworthy that the differences in these fluxes are larger for the inland region (60–80 W/m^2) compared to the coastal and Great Lakes urban regions (40–60 W/m^2). This shows the modulation effect of the adjoining water bodies on the urban climate. The distinctly enhanced diurnal cycle of the residual term in GEM_TEB can be noted because of the enhanced conduction of heat to soil layers during daytime and similarly to the atmosphere during nighttime. This higher nighttime near-surface temperature can also lead to lower relative humidity near the surface in GEM_TEB (not shown).

Figure 6 shows the diurnal distribution (in %) of summer precipitation simulated by GEM and GEM_TEB, which show important variations with region. It should be noted that only grid cells with urban fractions above 8 % are considered for analysis. For the coastal region, the distribution is bi-modal, while for the Great Lakes and inland regions, it is unimodal. Scaff et al. (2019) presents diurnal cycles of precipitation for various regions of North America; the results obtained with GEM and GEM_TEB follow the patterns in Scaff et al. (2019). Looking at the differences between the two experiments in detail, it is very noteworthy that GEM_TEB has relatively higher precipitation fraction during mid-day (11–16 LST) than GEM, irrespective of the sub-region. This implies that the higher temperatures in GEM_TEB contribute to strengthening convection during daytime and this result is similar to that reported in Manola et al. (2020). Therefore, for more advanced analysis related to this finding, short-duration precipitation extremes and related mechanisms are discussed in Sect. 3.2.

3.2 Impacts of urban regions on short-duration precipitation extremes

Figure 7 shows the simulated scalings of the 99th percentile of hourly precipitation intensity with respect to daily mean 2-m temperature for grid cells with urban fractions higher than 8 % for the three sub-regions. The geographic location of the sub-region has a strong influence on the simulated P-T relationship. However, the observed P-T relationship for all sub-regions show a peak-like structure, i.e. decreasing precipitation with temperature after the breaking point, where the highest precipitation intensities occur (Lenderink and Meijgaard 2010). In addition, the breaking points appear between 20 and 25 ºC, although it is slightly different depending on the sub-region. For the coastal and Great Lakes regions, super CC scaling (i.e., 14 % increase in precipitation per °C) between 10 and 15 ºC and then CC scaling (i.e., 7 % increase in precipitation per °C) are found until the breaking point. On the other hand, for the inland region, super CC scaling is noted until the breaking point, which means that inland region has a relatively stronger P-T relationship compared to the other sub-regions.

In general, the two experiments capture well the observed P-T relationship, although precipitation intensities are generally underestimated for all temperature bins compared to ERA5 data. When comparing the two experiments, GEM_TEB shows slightly lower precipitation intensities compared to

GEM experiment for the temperature bins up to the breaking point. Beyond the breaking point, GEM_TEB precipitation intensities are higher than that for GEM, for all sub-regions. These differences before and after the breaking point can be explained by the differences in the dominant precipitation generating mechanisms. Oh and Sushama (2020) in their study of short-duration precipitation extremes over the Canadian climatic regions using the same model demonstrated that, for low-temperature bins, the short-duration precipitation extremes are largely due to high relative humidity, while for high-temperature bins, strong convection due to atmospheric instability caused by surface warming is largely responsible. Therefore, lower precipitation intensities before the breaking point in GEM_TEB experiment can be explained by reduced evapotranspiration due to urban regions. On the other hand, higher precipitation intensities after the breaking point can be explained by enhanced convection brought by atmospheric instability due to higher urban temperatures.

For more detailed analysis, the spatial distribution of the differences in 99th percentile of hourly precipitation intensity between GEM_TEB and GEM beyond the breaking point for each grid cell is shown in Fig. 8. Differences in the atmospheric fields corresponding to the 99th percentile of hourly precipitation intensity beyond the breaking point are also shown; breaking points varies with grid cells and corresponds to the temperature bin with highest precipitation intensity. In general, higher precipitation intensities are noted in GEM_TEB compared to GEM for regions with higher urban fractions and their surrounding non-urban/rural regions, particularly for the coastal region. These regions of higher precipitation extremes in GEM_TEB compared to GEM are collocated with higher values of convective available potential energy (CAPE, J/kg) and cloud fraction (%). Interestingly, lower sea level pressure (hPa) is found around the coastal and Great Lakes regions in GEM_TEB compared with GEM, leading to enhanced sea and lake breeze, respectively, contributing additional water vapor to respective regions. Furthermore, the higher roughness length in GEM_TEB (Fig. S1) for these regions of high urban fractions can enhance mechanical turbulence, which when coupled with reinforced sea and lake breeze leads to dynamic convective development. Therefore, the higher cloud fraction for the urban regions and their surrounding non-urban/rural regions in GEM_TEB can be partly explained by the combined thermal and dynamic effects, which leads to higher precipitation extremes in these regions. This result is similar to that reported in Karlický et al. (2020) based on a multi-model ensemble over the European domain.

3.3 Impacts of urban regions on temperature extremes

Figure 9 shows the spatial distribution of the average number of heat-stress days per summer for both simulations and their differences. The fractional distribution of heat-stress events of varying durations for the three sub-regions are also presented. In general, 10 to 12 heat-stress days per summer are simulated by GEM. In the GEM_TEB experiment, the heat-stress days are higher by 3 days for grid cells with higher urban fraction than 8 %. These differences are found to be statistically significant at the 5 % significance level based on Student's t-test. This suggests that the urban regions can be subjected to more aggravated heat-stress conditions due to relatively higher temperatures despite the reduced relative humidity. Furthermore, higher urban temperatures, regardless of the sub-region, lead to more heat-stress events of longer duration (Fig. 9b). In particular, for coastal region, the number of heat-stress events lasting 6 days and above are found to be two times more in GEM_TEB compared to GEM. This result,

therefore, indicates that realistic representation of urban regions in climate models is critical to better simulate the duration and frequency of temperature extremes.

Figure 10 shows the box-whisker plots for the start and end dates of the first and last heat-stress events over urban grid cells defined for the three sub-regions, respectively, for the 1981–2010 period. In general, the median values for the start and end dates vary with sub-region but the start (end) date for all sub-regions appear to be positively (negatively) skewed. The coastal (inland) region shows an early (later) start and later (early) end to the heat-stress season, compared to other sub-regions. This implies that the start and end dates of the heat-stress season are related to the climatic characteristics of the sub-region. In the GEM_TEB experiment, the higher urban temperatures lead to the relatively longer heat-stress season compared to GEM experiment. In particular, the heat-stress season is longer for the inland region compared to the other two sub-regions.

4 Summary And Conclusion

This study assesses the urban-climate interactions during summer for eastern North America using regional climate model simulations at 0.22° resolution for the 1981–2010 period. To this end, two experiments are set up using the limited area version of the GEM model with and without TEB scheme for urban fractions (named as GEM_TEB and GEM, respectively). To study the influence of geographic location on urban-climate interactions, three sub-regions –coastal, Great Lakes, and inland regions – are considered.

In general, GEM_TEB simulates higher temperatures and reduced precipitation for the urban regions by around 0.7 ºC and 0.3–0.5 mm/day, respectively, compared to GEM experiment, generally contributing to model improvements for both variables compared to observations, except for urban gird cells with a warm bias in GEM. These differences are related to lower albedo and soil moisture, respectively, in GEM_TEB for urban regions/cells, which lead to higher absorbed solar radiation at the surface during daytime and therefore higher sensible heat flux but smaller latent heat flux. These differences in energy fluxes are larger for the inland region than for the coastal and Great Lakes regions, indicating that the ocean and lake adjacent to urban regions modulate the urban climate system.

Interestingly, GEM_TEB has relatively higher precipitation fraction during mid-day (11–16 LST) than GEM, irrespective of the sub-region, suggesting that higher urban temperatures in GEM_TEB contribute to strengthening convection during daytime. For example, the 99th percentile of hourly precipitation intensity for high-temperature bins in GEM_TEB are higher than that for GEM, particularly for the coastal and Great Lakes regions. These higher precipitation extremes are collocated with higher values of convective available potential energy (CAPE, J/kg) and cloud fraction (%). In addition, enhanced sea and lake breezes with lower sea level pressure (hPa) in GEM_TEB are found around these regions, leading to additional water vapor and dynamic convective development. Therefore, the higher cloud fraction for the urban regions and their surrounding non-urban/rural regions in GEM_TEB can be attributed to the combined enhanced thermal and dynamic effects, which leads to higher precipitation extremes in these

regions. Analysis of temperature extremes suggests that the urban regions can be subjected to more aggravated heat-stress conditions due to relatively higher temperatures, despite reduced relative humidity. For example, double the number of extreme heat spells lasting 6 or more days for the coastal urban region are simulated in GEM_TEB compared to GEM. Furthermore, longer heat-stress season is simulated by GEM_TEB.

This study demonstrates the added-value of improved representation of urban regions in the regional climate model, particularly in the simulation of mean climate and selected extremes. In addition, this study shows distinct conflicting urban effects on precipitation: (1) reduced evapotranspiration leading to reduced precipitation and (2) enhanced thermal and dynamic convections triggering increased precipitation which is clearly noticeable for short-duration precipitation extremes at higher temperatures. This study provides the basis for future studies focussed on transient climate simulations using the GEM_TEB configuration, which are required to assess changes to urban mean and extreme climates, with a high level of confidence.

Declarations

Acknowledgments

The first author would like to thank Vincent Poitras and Bernardo Teufel with the processing of the urban geophysical fields. The GEM simulations considered in this study were performed on the supercomputer managed by Compute Canada and Calcul Québec. Model output data and analysis data for this study are available for request to the corresponding author (seokgeunoh@snu.ac.kr).

References

Balk, D. L., Deichmann, U., Yetman, G., Pozzi, F., Hay, S. I., Nelson, A., 2006. Determining global population distribution: method, application and data. Adv. Parasitol. 119–156.

Bélair S, Leroyer S, Seino N, Spacek L, Souvanlasy V, Paouin-Ricard D (2018) Role and impact of the urban environment in a numerical forecast of an intense summertime precipitation event over Tokyo. J Meteorol Soc Japan 96A:77–94

Bélair S, Mailhot J, Girard C, Vaillancourt P (2005) Boundary layer and shallow cumulus coulds in a medium-range forecast of a large-scale weather system. Mon Wea Rev 133:1938–1960

Benoit R, Cote J, Mailhot J (1989) Inclusion of a Tke boundary-layer parameterization in the Canadian regional finite-element model. Mon Wea Rev 117(8):1726–1750

Cha DH et al (2016) Future changes in summer precipitation in regional climate simulations over the Korean Peninsula forced by multi-RCP scenarios of HadGEM2-AO. Asia-Pacific J Atmos Sci 52:139–149

Cote J, Gravel S, Methot A, Patoine A, Roch M, Staniforth A (1998) The operational CMC-MRB global environmental multiscale (GEM) model. Part I: design considerations and formulation. Mon Wea Rev 126(6):1373–1395

Daniel M, Lemonsu A, Deque M, Somot S, Alias A, Masson V (2019) Benefits of explicit urban parameterization in regional climate modeling to study climate and city interactions. Clim Dyn 52:2745–2764

Dee DP et al (2011) The ERA-Interim reanalysis: configuration and performance of the data assimilation system. Q J R Meteorol Soc 137(656):553–597.

Delage Y (1997) Parameterising sub-grid scale vertical transport in atmospheric models under statistically stable conditions. Boundary-Layer Meteorol 82:23–48

Hamdi R, Degrauwe D, Termonia P (2012) Coupling the town energy balance (TEB) scheme to an operational limited-area NWP model: Evaluation for a highly urbanized area in Belgium. Weather Forecast 27:323–344

Hersbach H et al. (2020) The ERA5 global reanalysis. Q J R Meteorol Soc., https://doi.org/10.1002/qj.3803

Huszar P, Halenka T, Belda M, Zak M, Sindelarova K, Miksovsky J (2014) Regional climate model assessment of the urban land-surface forcing over central Europe. Atmos Chem Phy 14:12393–12413

IPCC (2007), Climate Change 2007. In the physical science basis. Contribution of working group I to the fourth assessment report of the Intergovernmental Panel on Climate Change, S. Solomon, D. Qin, M. Manning, Z. Chen, M. Marquis, K. B. Averyt, M. Tignor, H. L. Miller (eds). Cambridge University Press: Cambridge, United Kingdom and New York, NY, USA, p996

Jeong DI, Sushama L (2016) Projected changes to high temperature events for Canada based on a regional climate model ensemble. Clim Dyn 46:3163–3180

Kain JS, Fritsch JM (1992) The role of the convective “trigger function” in numerical forecasts of mesoscale convective system. Meteorol Atmos Phy 49:93–106

Karlicky J et al (2018) Multi-model comparison of urban heat island modelling approaches. Atmos Chem Phy 18:10655–10674

Karlicky J et al (2020) The urban meteorology island: a multi-model ensemble analysis. Atmos Chem Phys Discuss., https://doi.org/10.5194/acp-2020-433

Lenderink G, van Meijgaard E (2010) Linking increases in hourly precipitation extremes to atmospheric temperature and moisture changes. Environ Res Lett. https://doi.org/10.1088/1748-9326/5/2/025208

Leroyer S, Bélair S, Mailhot J, Strachan IB (2011) Microscale numerical prediction over Montreal with the Canadian external urban modeling system. J Appl Meteorol Climatol 50:2410–2428

Li J, Barker HW (2005) A radiation algorithm with correlated-k distribution. Part I: local thermal equilibrium. J Atmos Sci 62(2):286–309

Li XX, Koh TY, Panda J, Norford LK (2016) Impact of urbanization patterns on the local climate of a tropical city, Singapore: an ensemble study. J Geophys Res Atmos 121:4386–4403

Manola et al. (2020) Analysis of urban rainfall from hourly to seasonal scales using high-resolution radar observations in the Netherlands. Int J Climatol 40:822–840

Martynov A, Laprise R, Sushama L, Winger K, Separovic L, Dugas B (2013) Reanalysis-driven climate simulation over CORDEX North America domain using the Canadian regional climate model, version 5: model performance evaluation. Clim Dyn. https://doi.org/10.1007/s00382-013-1778-9

Masson V (2000) A physically-based scheme for the urban energy budget in atmospheric models. Boundary-Layer Meteorol 94:357–3970

Masson V, Grimmond CSB, Oke TR (2002) Evaluation of the town energy balance (TEB) scheme with direct measurements from dry district in two cities. J Appl Meteorol 41:1011–1026

McCarthy MP, Best MJ, Betts RA (2010) Climate change in cities due to global warming and urban effects. Geophy Res Lett. https://doi.org/10.1029/2010GL042845

Miao S, Dou J, Chen F, Li J, Li A (2012) Analysis of observations on the urban surface energy balance in Beijing. Sci. China Earth Sci. 55(11):1881–1890

Molders N, Olson MA (2004) Impact of urban effects on precipitation in high latitutes. J Hydrometeorol 5:409–429

Nazarnia N, Schwick C, Jaeger J (2016) Accelerated urban sprawl in Montreal, Quebec City: and Zurich: investigating the differences using time series 1951 2011. Ecol Indic 60:1229–1251

Oh SG, Sushama L (2020) Short-duration precipitation extremes characteristics over Canada in a warmer climate. Clim Dyn 54(3):2493–2509

Oke TR (1982) The energetic basis of the urban heat island. Q J R Meteorol Soc 108:1–24

Oke TR (1988) The urban energy balance. Prog Phys Geogr 12:471–508

Oleson KW, Bonan GB, Feddema J, Jackson T (2011) An examination of urban heat island characteristics in a global climate model. Int J Climatol 31:1848–1865

Oleson KW (2012) Contrasts between urban and rural climate in CCSM4 CMIP5 climate change scenarios. J Clim 25:1390–1412

Oleson KW et al (2015) Interactions between urbanization, heat stress, and climate change. Climatic Change 129:525–541

Roberge F, Sushama L (2018) Urban heat island in current and future climates for the island of Montreal. Sustain Cities Soc 40:501–512

Scaff L, Prein AF, Li Y, Liu C, Rasmussen R, Ikeda K (2019) Simulating the convective precipitation diurnal cycle in North America's current and future climate. Clim Dyn. https://doi.org/1.1007/s00382-019-04757-9

Shepherd JM, Burian SJ (2003), Detection of urban-induced rainfall anomalies in a major coastal city. Earth Interact 7:1–17

Smoyer KE (1998) A comparative analysis of heat waves and associated mortality in St. Louis, Missouri – 1980 and 1995. Int J Biometeorol 42:44–50

Steadman RG (1984) A universal scale of apparent temperature. J Clim Appl Meteorol 23:1674–1687

Steinweg C, Gutowski WJ (2015) Projected changes in greater St. Louis summer heat stress in NARCCAP simulation. Weather Clim Soc 7:159–168

Sundqvist H, Berge E, Kristjánsson JE (1989) Condensation and cloud parameterization studies with a mesoscale numerical weather prediction model. Mon Wea Rev 117:1641–1657

Teufel B et al (2017) Investigation of the 2013 Alberta flood from weather and climate perspectives. Clim Dyn 48:2881–2899

Thornton PE et al (2017) Daymet: Daily surface water data on a 1 km grid for North America, version 3, ORNL DAAC, Oak Ridge, Tennessee, USA. https://doi.org/10.3334/ORNLDAAC/1328

Yeh KS, Cote J, Gravel S, Methot A, Patoine A, Roch M, Staniforth A (2002) The CMC-MRB global environmental multiscale (GEM) model. Part III: Nonhydrostatic formulation. Mon Wea Rev 130(2):339–356

Verseghy DL (2009) CLASS-The Canadian land surface scheme (version 3.4)-technical documentation (version 1.1). Internal report, Climate Research Division, Science and Technology Branch, Environment Canada, p183

Wang D, Jiang P, Wang G, Wang D (2015) Urban extent enhances extreme precipitation over the Pearl River Delta, China. Atmos Sci Lett 16:310–317

Zadra A, McTaggart-Cowan R, Roch M (2012) Recent changes to the orographic blocking. Seminar presentation, PRN, Dorval, Canada, 30 March 2012. http://collaboration.cmc.ec.gc.ca/science/rpn/SEM/dossiers/2012/seminaires/2012-03-30/Seminar_2012-03-30_Ayrton-Zadra.pdf, Accessed 27 Aug. 2018

Zhang H, Wu C, Chen W, Huang G (2019) Effect of urban expansion on summer rainfall in the Pearl River Delta, South China. J. Hydrol 568:747–757

Figures

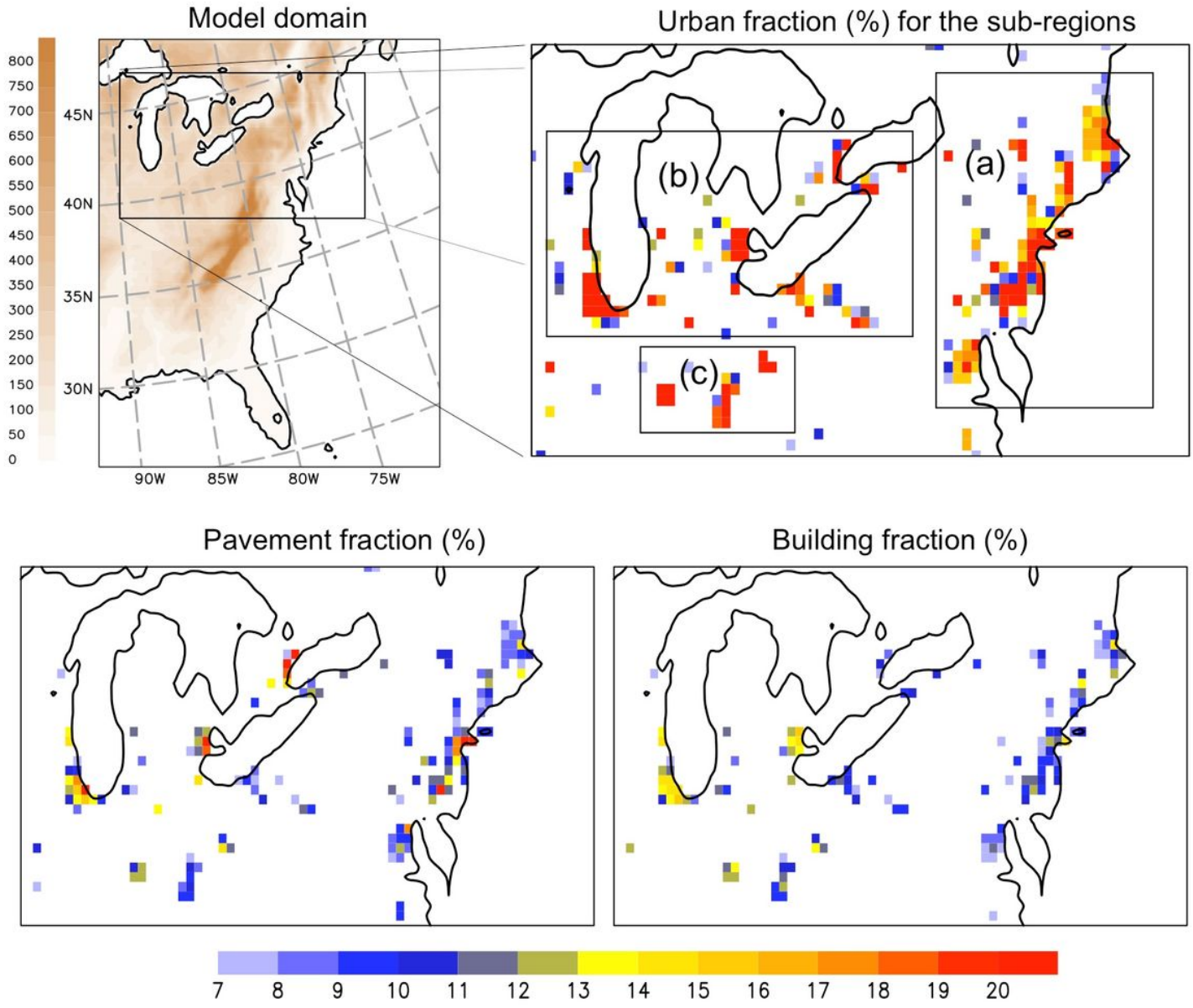

Figure 1

Model domain (excluding blending and halo zones) with topography (in m; left panel) at 0.22° horizontal resolution. The three sub-regions (coastal, Great Lakes and inland regions) used for detailed analysis and

urban fractions (in %; upper-right panel). The pavement and building fractions (%) over the study domain (lower panels).

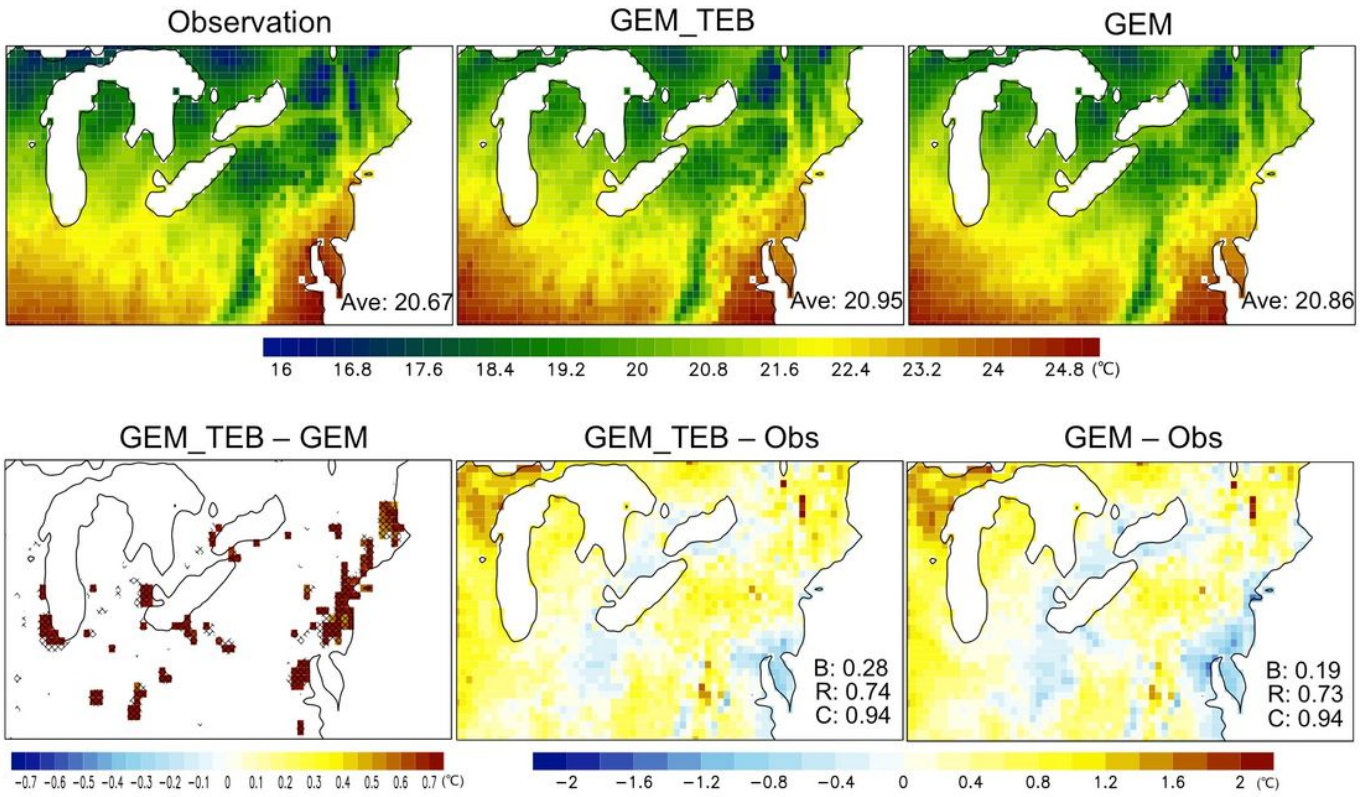

Figure 2

Spatial distribution of the observed and modelled mean summer (JJA) 2-m temperature (ºC) for the 1981–2010 period. The differences between experiments and observation and between the two experiments GEM_TEB and GEM are also presented. The area-averaged value (Ave.) of each dataset and the bias (B), root mean square error (R), and correlation (C) for the two simulations compared to observation are also indicated in respective figures. For the difference between two experiments (GEM_TEB minus GEM), only statistically significant differences (at 5 % significance level of the Student's t-test) are shown and the grid cells shown hatched have urban fraction higher than 8 %.

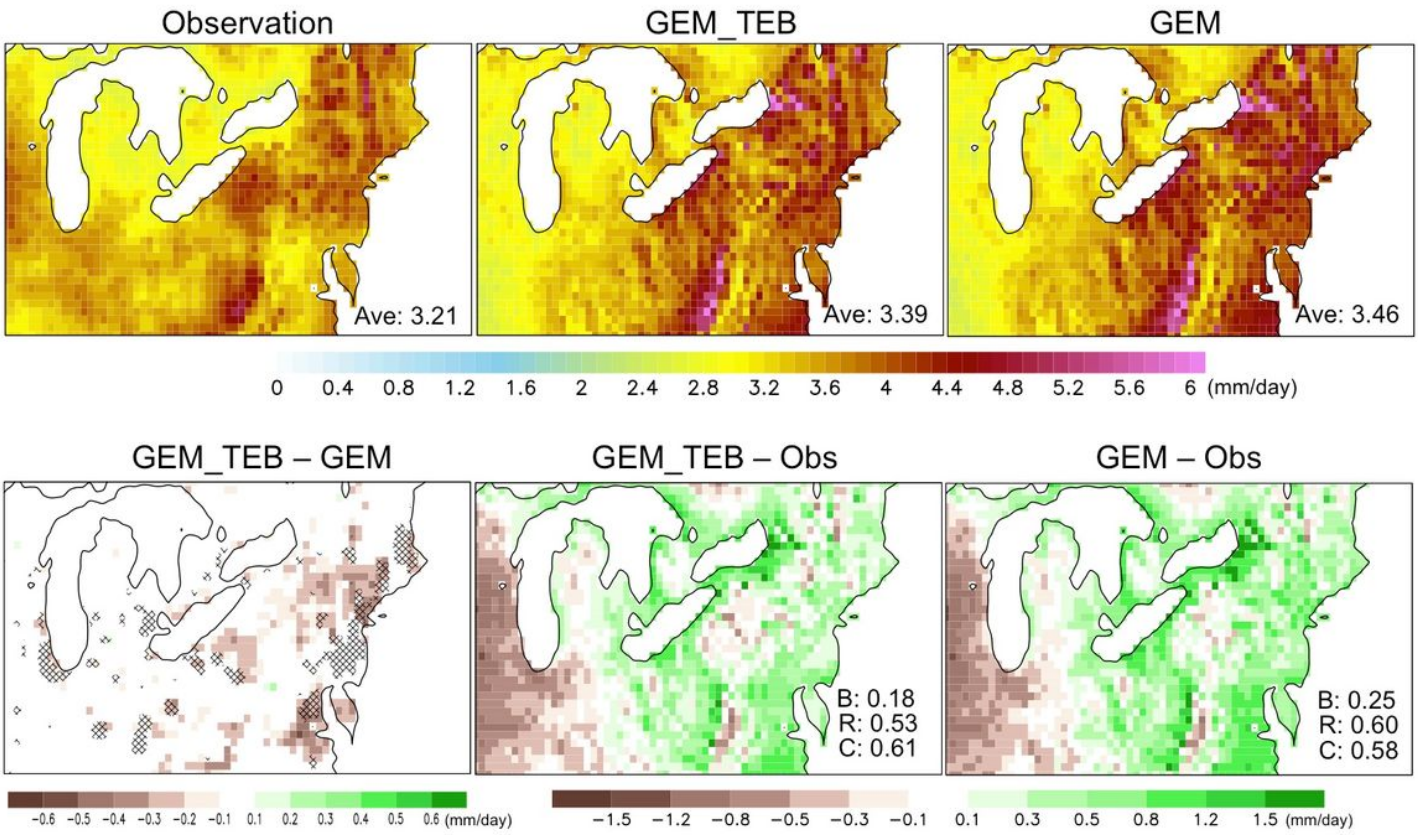

Figure 3

Same as Fig. 2, but for summer precipitation (mm/day).

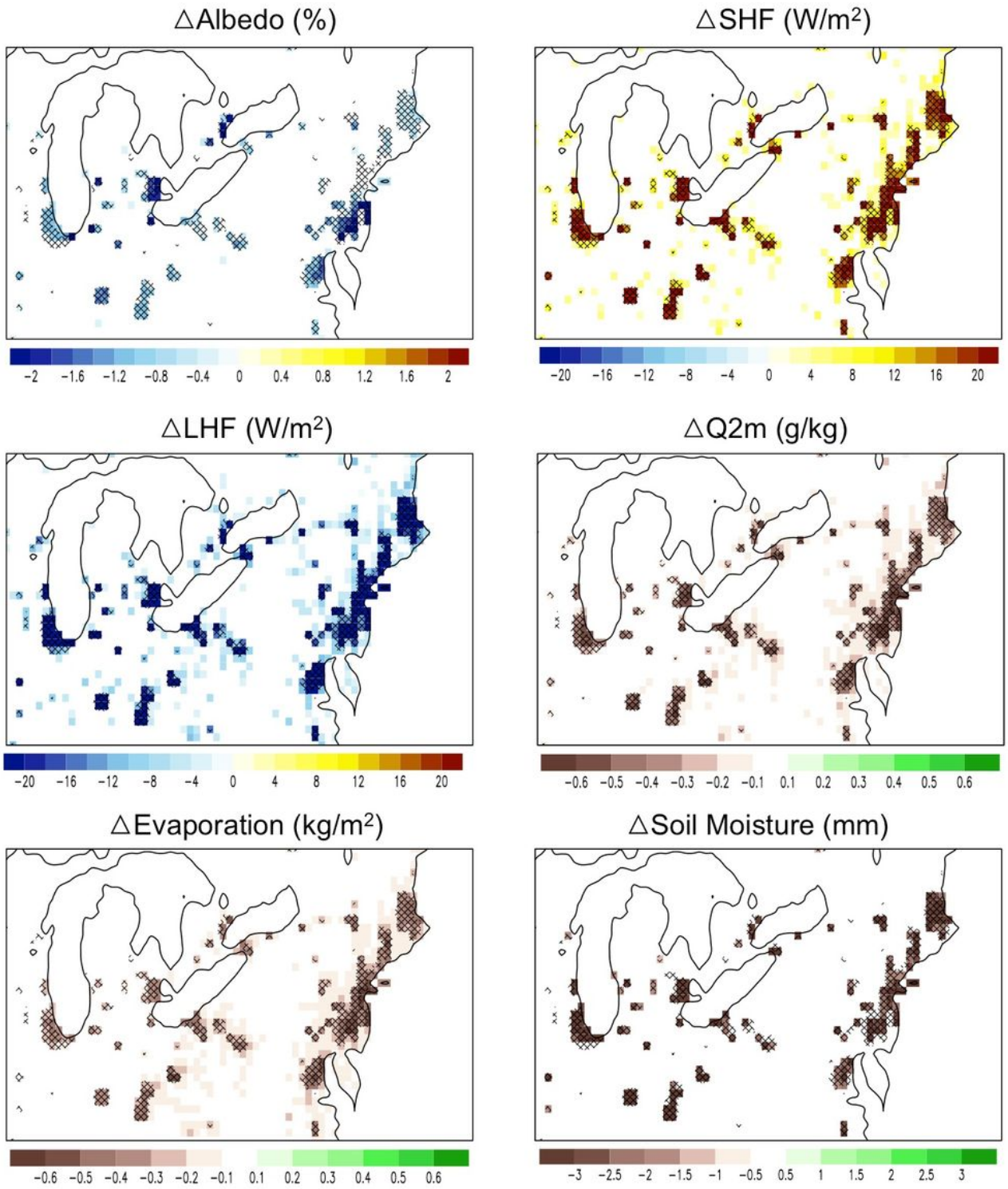

Figure 4

Spatial distribution of the difference (GEM_TEB minus GEM) in summer albedo, sensible heat flux (SHF), latent heat flux (LHF), 2-m specific humidity (Q2m), evaporation, and soil moisture for the 1981–2010 period. Only grid cells with statistically significant differences obtained with Student's t-test at 5 % significance level are shown. Grid cells shown hatched have urban fraction higher than 8 %.

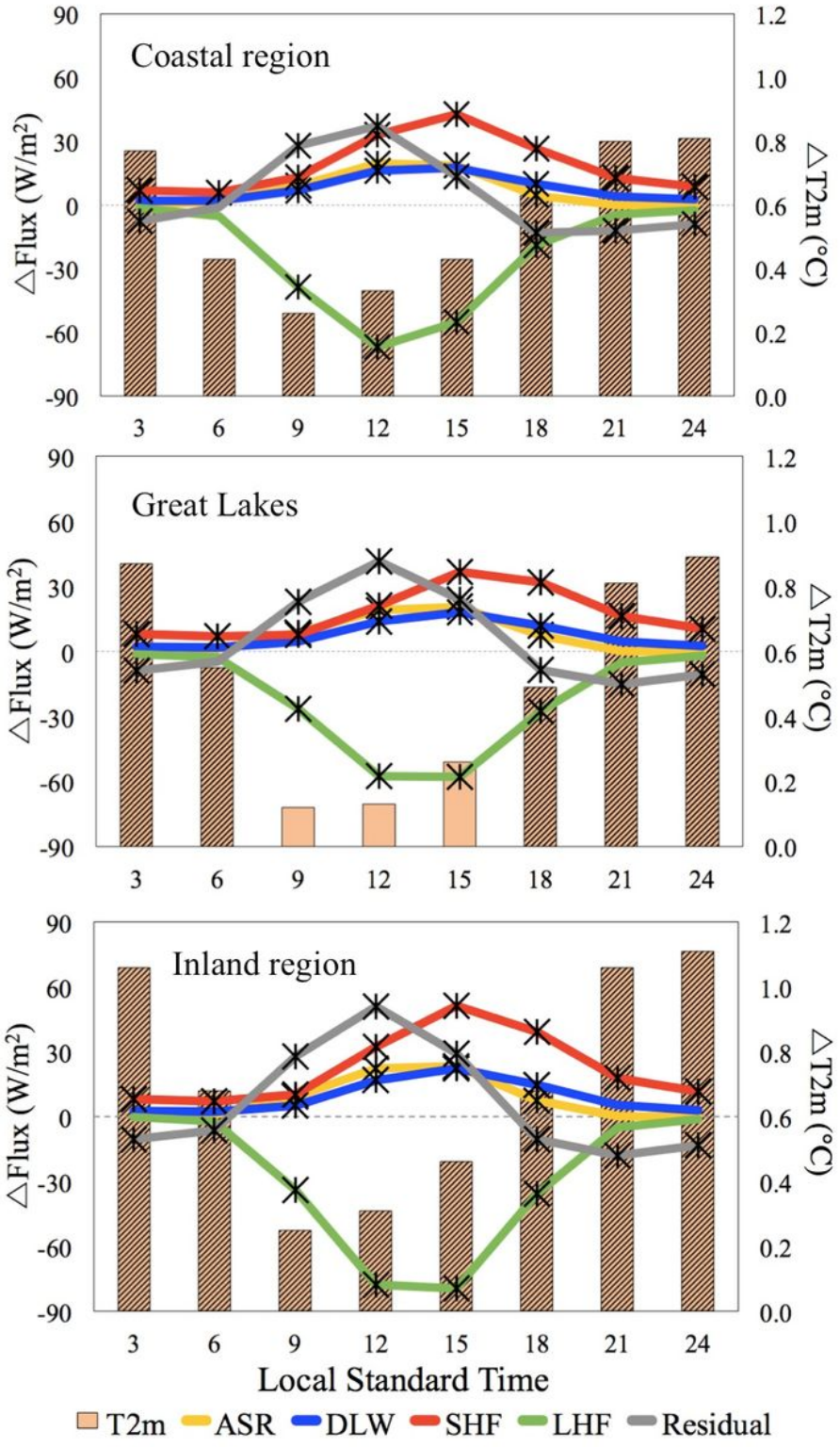

Figure 5

Differences in the diurnal cycle of surface 2-m temperature (T2m) and surface energy budget between GEM_TEB and GEM experiments for summer for the 1981–2010 period. Note that ASR, DLW, SHF, LHF indicate the absorbed solar radiation, downward longwave radiation, sensible heat flux, and latent heat flux, respectively. Based on assumption which the heat storage is zero for an infinitely thin surface layer, the residual term in this study is estimated as the difference between the net radiative and turbulent

fluxes which are explicitly provided in model output. Only grid cells with urban fractions above 8 % are used in constructing these plots. The asterisk, in the case of line plots, and hatched bars indicate statistically significant differences with Student's t-test at 5 % significance level.

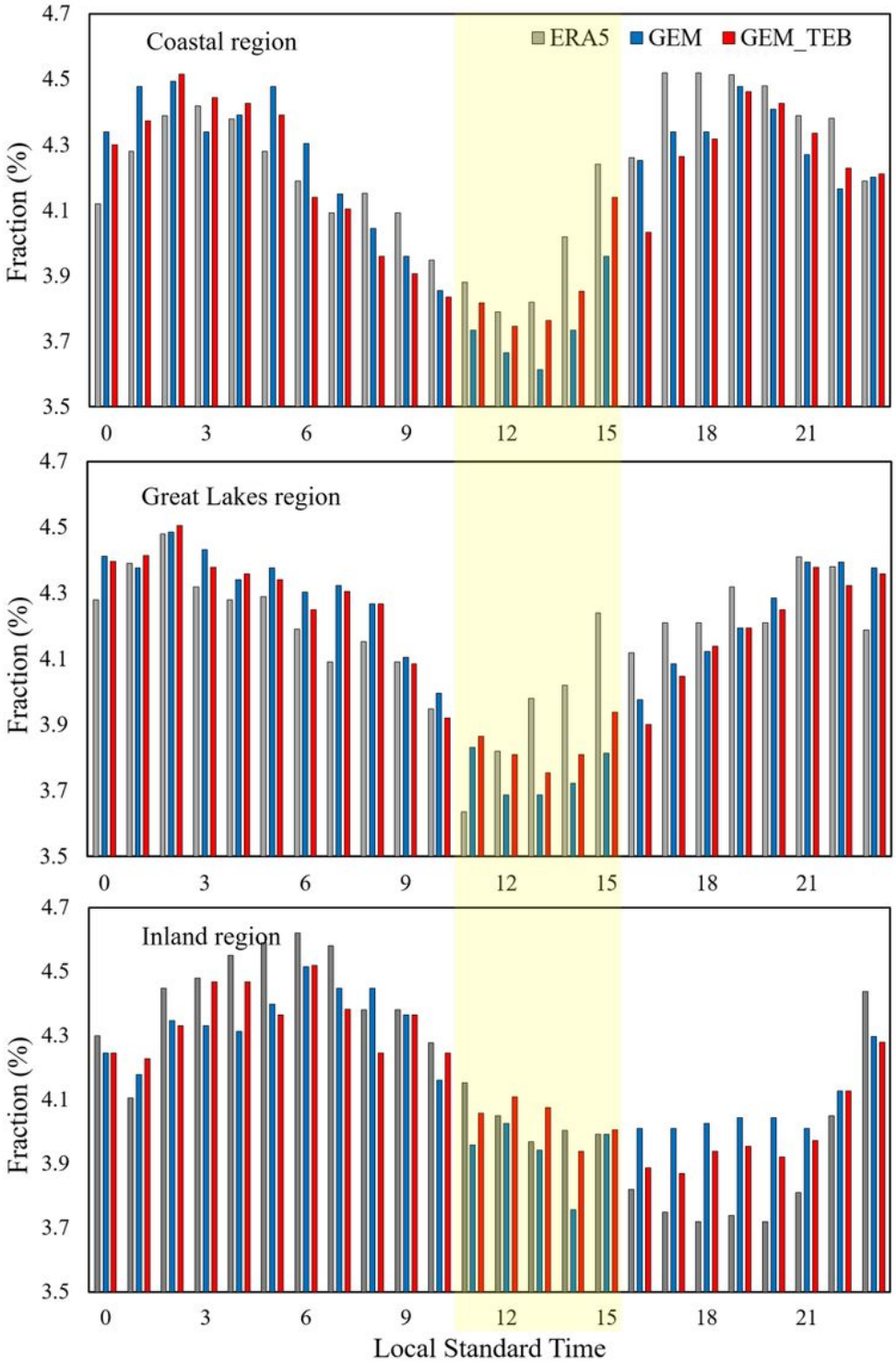

Figure 6

Daily distribution (%) of precipitation for summer for the 1981–2010 period for ERA5, GEM, and GEM_TEB experiments. The time interval from 11 to 16 local standard time (LST) is shown shaded in

yellow. This fractional value is calculated as the ratio of the accumulated precipitation amount for each time interval to the daily accumulated precipitation amount for the 1981–2010 period.

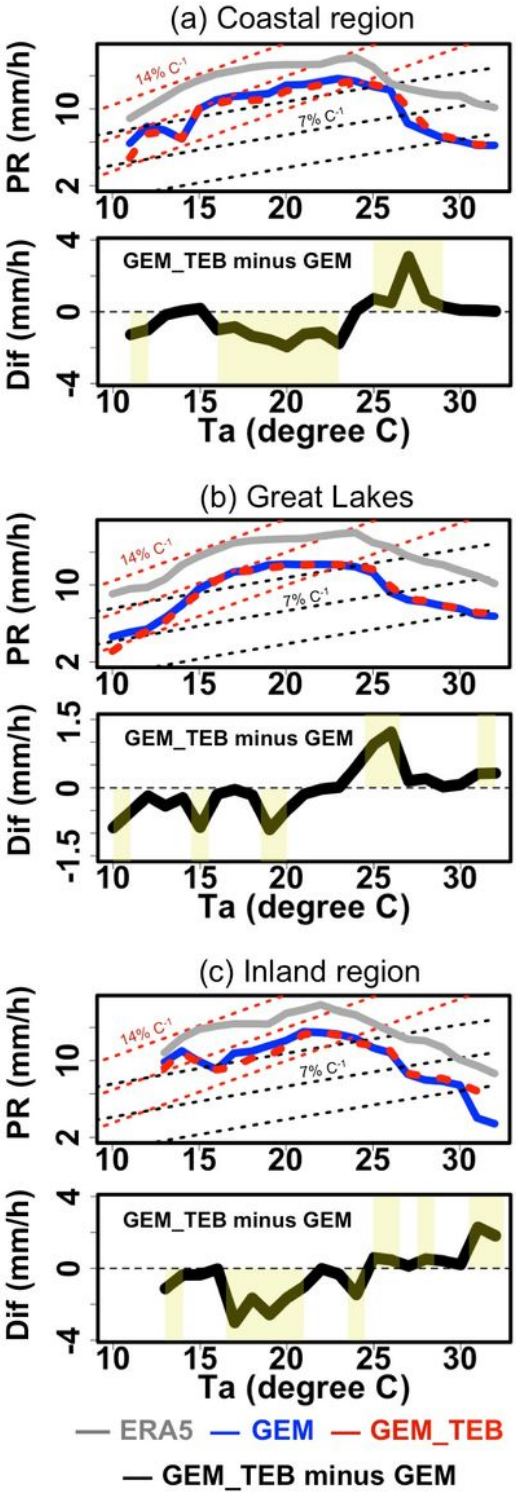

Figure 7

The simulated 99th percentile of hourly precipitation - daily mean 2-m temperature (P-T) relationship for the three sub-regions considered in this study for the 1981–2010 period. Bottom panel of each sub-plot shows the difference in the P-T relationship between GEM_TEB and GEM experiments. Statistically

significant differences at 5 % significance level obtained with Student's t-test is shown shaded in yellow. The black and red dotted lines in the upper panel of each sub-plot correspond to 7 % °C-1 and 14 % °C-1, respectively.

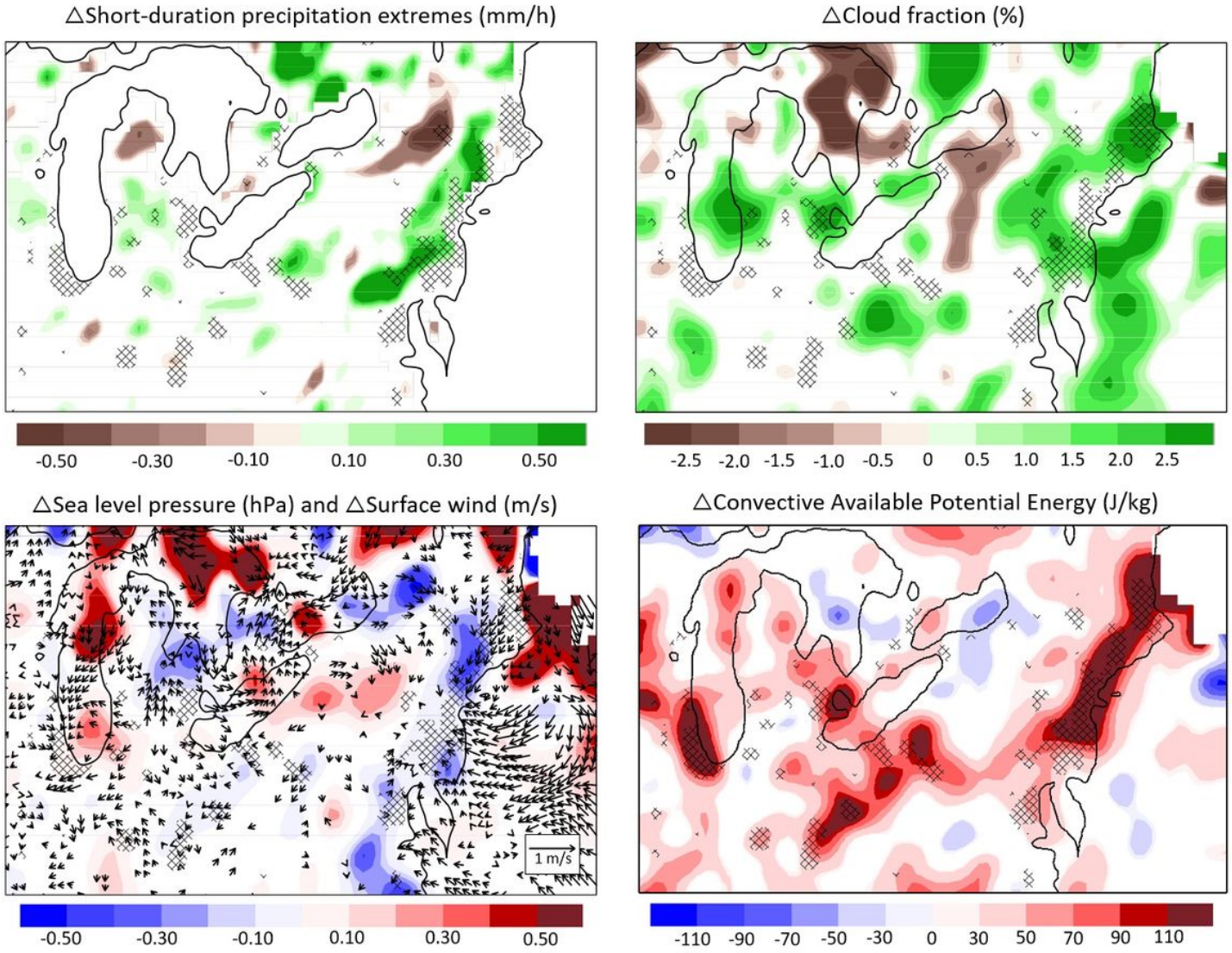

Figure 8

Spatial distribution of the difference between GEM_TEB and GEM experiments for the 99th percentile of hourly precipitation (mm/h) after the breaking point for the 1981–2010 period. The differences in cloud fraction (%), sea level pressure (hPa), with surface wind vector (m/s), and convective available potential energy (J/kg) associated with the 99th percentile of hourly precipitation are also presented. The grid cells shown hatched have urban fractions higher than 8 %. Only statistically significant differences at 5 % significance level obtained with the Student's t-test are shown.

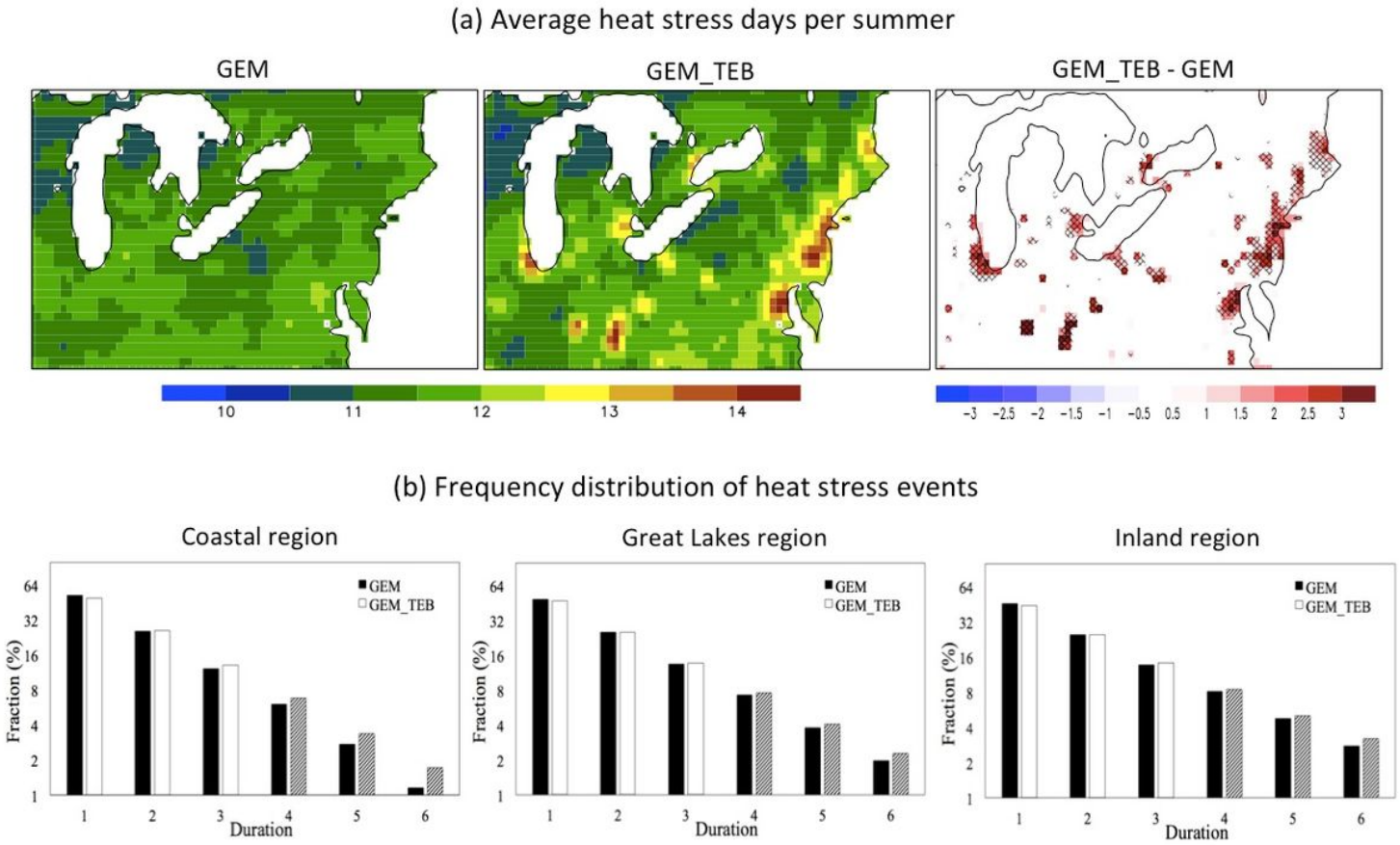

Figure 9

(a) Spatial distribution of mean number of heat-stress days per summer as simulated by GEM_TEB and GEM experiments and their difference; only grid cells with statistically significant differences obtained with Student's t-test at 5 % significance level are shown in the latter plot. (b) Fractional distribution of heat-stress events of varying durations for the three studied sub-regions. This fractional value is calculated as the ratio of heat-stress events for each duration to total heat-stress events for 1981–2010. The hatched bars in Fig. 9b indicate statistically significant differences between GEM_TEB and GEM at 5 % significance level obtained with the Z-test.

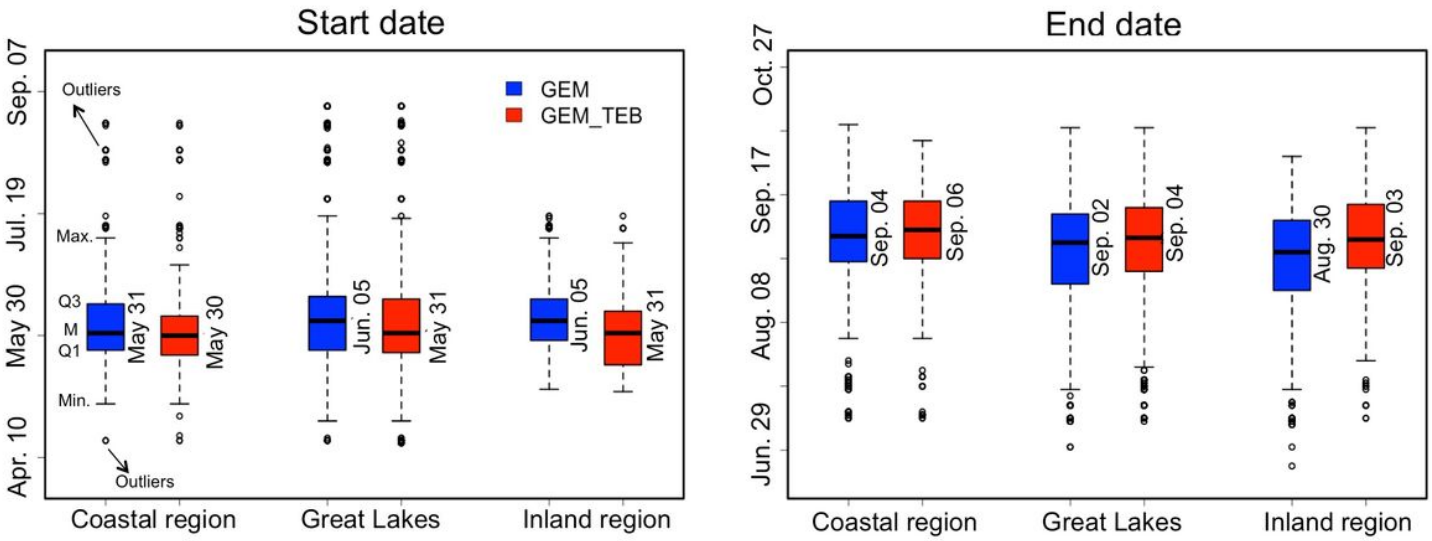

Figure 10

Box and whisker plots for the start and end dates of the first and last heat-stress events, respectively, for the 1981–2010 summer period. Six-number summary of box plot is also shown; minimum score (Min.), 25th percentile (Q1), median (M), 75th percentile (Q3), maximum score (Max.), and outliers (circle).

Supplementary Files

This is a list of supplementary files associated with this preprint. Click to download.

- SupplementaryMaterials.pdf